Physics of Fluids

An extended model for orifice starting jets

Cite as: Phys. Fluids **33**, 067109 (2021); https://doi.org/10.1063/5.0048813
Submitted: 26 February 2021 • Accepted: 09 May 2021 • Published Online: 14 June 2021

Raphaël Limbourg and Jovan Nedić

Physics of Fluids ARTICLE scitation.org/journal/phf

An extended model for orifice starting jets

Cite as: Phys. Fluids **33**, 067109 (2021); doi: 10.1063/5.0048813
Submitted: 26 February 2021 · Accepted: 9 May 2021 ·
Published Online: 14 June 2021

Raphaël Limbourg and Jovan Nedić[a)]

AFFILIATIONS

Department of Mechanical Engineering, McGill University, Montréal, Québec H3A 0C3, Canada

[a)]Author to whom correspondence should be addressed: jovan.nedic@mcgill.ca

ABSTRACT

Starting jets emanating from a straight nozzle and orifices of different orifice-to-tube diameter ratios are investigated using time-resolved particle image velocimetry. The invariants of the motion, namely, the circulation, the hydrodynamic impulse, and the kinetic energy, are measured and compared to the classic slug-flow model, and this for both fixed exhaust speed and fixed diameter-based Reynolds numbers. An extension to the slug-flow model is proposed to account for the contraction the fluid is experiencing when being pushed out through orifice geometries. The contraction coefficients obtained for two-dimensional jets formed through a slit in a channel are applied to the axisymmetric problem. This modified slug-flow model is shown to better predict the invariants of the motion with discrepancies of the order of 10% compared to underpredictions of 130%, 50%, and 120% for the circulation, the hydrodynamic impulse, and the kinetic energy, respectively, using the classic slug-flow model. Moreover, for a fixed target exhaust speed, the model suggests the existence of a maximum in the production of impulse and energy at an orifice-to-tube diameter ratio of about 0.9, which was also observed experimentally for the kinetic energy. Practically speaking, this suggests that the most efficient way of producing a starting jet is using an orifice plate of ratio close to 1, but different from a straight nozzle. Finally, the overpressure correction of Krueger ["The significance of vortex ring formation and nozzle exit overpressure to pulsatile jet propulsion," Ph.D. thesis (California Institute of Technology, 2001)] is applied and revisited to account for the orifice-to-tube diameter ratio. Overall, good agreement with the present experimental data is found.

I. INTRODUCTION

Starting jets can be classified into two categories: parallel or converging starting jets, in which the boundary layer inside the tube thickens in time, and orifice starting jets consisting of a thin orifice plate covering the exhaust of a straight tube (see Fig. 1). Synthetic (zero-net mass flux) jets and pulsed jets, both being periodically starting jets, have proved their utility in regard to flow control and mixing. The production of such jets is inherently accompanied by the formation of a discrete train of vortices. One popular design for generating synthetic jets consists of an orifice plate covering a sealed cavity in which the flow is driven by a diaphragm or a piston.[2] Moreover, the formation process of orifice-generated vortex rings was shown to differ from the well-documented nozzle geometry case. In particular, Krieg and Mohseni,[3,4] corroborated and complemented by Limbourg and Nedić,[5] showed that orifice starting jets produce more circulation, hydrodynamic impulse, and kinetic energy than the equivalent parallel starting jet; the difference was attributed to the radial component of velocity at the lip of the orifice, which, in the case of a nozzle geometry, remains negligible throughout the process. Additionally, the absence of a boundary layer modifies the formation and growth of the leading vortex ring, and thus the production of the invariants of the motion.

In order to model the production of circulation of a parallel starting jet, Didden[6] proposed a model that assumes the flow to be a uniform slug of fluid with parallel streamlines. This slug-flow model was extended upon the prediction of the hydrodynamic impulse and the kinetic energy by Gharib *et al.*[7] The model was found to provide an adequate approximation of the total invariants of the motion generated by a nozzle, with differences of the order of 30% for circulation.[3] An effort was made to reduce the discrepancy with the model by considering secondary effects highlighted by Didden.[6] In particular, a boundary layer correction was proposed by Shusser *et al.*,[8] revised by Dabiri and Gharib,[9] to account for the thickening of the laminar boundary layer inside the tube. The model rests upon the unsteady laminar boundary layer growth over a semi-infinite flat plate impulsively started from rest (Stokes' first problem). Later, an overpressure correction was proposed by Krueger;[1,10–12] applied to both nozzle and orifice geometries, the additional circulation was found to be proportional to the product of the exhaust speed and the exhaust diameter. Moreover, in the case of an orifice geometry of orifice-to-tube diameter ratio tending to zero, Krueger[10] modeled the centerline velocity to be increased during ejection due to the creation of a *vena contracta*. The model was proved to enhance the prediction of the slug-flow

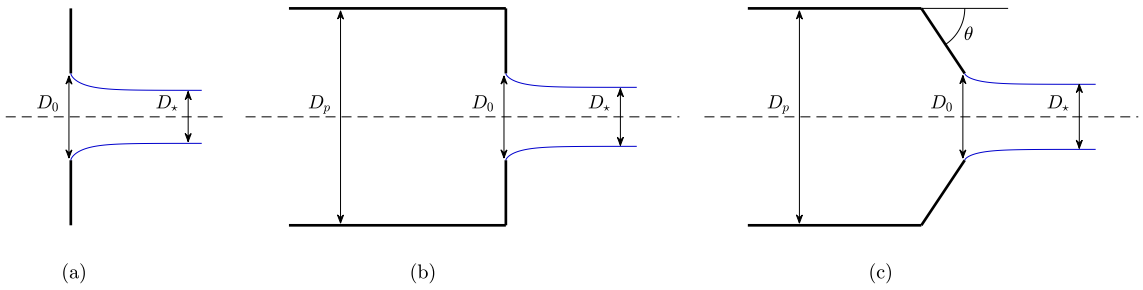

FIG. 1. Starting jets emanating from (a) an orifice in a plane (b) an orifice in a straight tube (c) a converging nozzle. Schematics made to scale.

model with discrepancies reduced to about 10%, when compared with simulations of laminar starting jets.[11,12] Finally, Krieg and Mohseni[3] proposed a semi-empirical model that accounts for the unsteadiness of the axial velocity and the nonzero radial velocity of orifice starting jets. However, the latter model necessitates the knowledge of experimental parameters, such as the velocity profile, which thus limits its use to an *a posteriori* analysis.

None of these models, however, address the contraction the flow is experiencing when exiting orifices of different orifice-to-tube diameter ratios D_0/D_p. The steady jet of fluid exiting a large vessel is a classic problem in hydrodynamics.[13–16] Of interest is the contraction coefficient C_c, defined as the ratio of the area of the contracted section $A_\star$, called *vena contracta*, mathematically at infinity downstream, to the exhaust area A_0, i.e., $C_c = A_\star/A_0$ (Fig. 1). For a two-dimensional slot in an infinite plane, the problem of finding the free streamline emanating from the exhaust was first solved by Kirchhoff[17] who found the contraction coefficient to be $C_c = \pi/(\pi + 2) \approx 0.611$ [Fig. 1(a)]. For a two-dimensional flow exiting a large vessel through a channel, one is left with the classic two-dimensional problem of Borda's mouthpiece,[18] first solved by means of the theory of free streamlines by von Helmholtz.[19] Finally, for a slot in a channel, with or without a conical exhaust [Figs. 1(b) and 1(c)], the problem was solved in a comprehensive manner by Von Mises,[20] and this for different orifice-to-tube diameter ratios D_0/D_p.

If the use of conformal mapping and complex variables makes the rectilinear two-dimensional problem easy to solve, the axisymmetric problem is a much harder problem and one must rely on approximate methods. The problem of finding the coordinates of the free streamline emanating from a circular hole in an infinitely large vessel was first solved by Trefftz[21] who modeled the jet efflux by sources and dipoles distributed over the surface of an infinitely large vessel. This results in a Fredholm integral equation of the second kind, of unknown the velocity potential, which was then solved using a trial and error procedure. Surprisingly, the contraction coefficient was found to be very close, nay identical, to the one found by Kirchhoff[17] for the two-dimensional problem. Later, Southwell and Vaisey[22] applied a relaxation method to the case of an orifice of ratio 1–6, compared to the cylindrical vessel, and found a value of 0.608, thus corroborating the results of Trefftz.[21] Finally, Rouse and Abul-Fetouh[23] tried to refine the result of Trefftz[21] using a relaxation method and ultimately found very similar results as the original conclusions of Trefftz.[21] Besides, Rouse and Abul-Fetouh[23] compared their numerical results and some experimental results from the literature with the analytical results of Von Mises[20] for the equivalent two-dimensional problem. Again, minor differences were found, hence concluding on the validity and the applicability of the two-dimensional analytical results for the three-dimensional problem. Furthermore, Salamatov[24] showed that the contraction coefficient of an infinitely large conical vessel of angle 40° is about 0.75, close to the value of 0.77 of Von Mises[20] for a two-dimensional flow; this was obtained by modeling the conical vessel as successive vortex rings.

Later, Garabedian[25] put into question the well-accepted result of Trefftz[21] and a rigorous mathematical method was developed to find the free streamline of the jet emanating from an orifice in an infinite plane wall. A contraction coefficient noticeably different from previous investigations was found with a value $C_c = 0.58$. Hunt,[26] in an attempt to close the debate, used a vortex representation of the interior surface which leads directly to the Fredholm integral equation of the second kind. The equation was solved numerically and the contraction coefficients for orifice-to-tube area ratios of 0.00, 0.25, 0.50, and 0.75 were computed. In particular, a contraction coefficient of $C_c = 0.578$ was found for an orifice in an infinite plane, close to Garabedian's[25] results, but in contradiction with experiments. Finally, Jeppson[27] used an inverse finite-difference formulation and found the free streamline emanating from a large vessel to be close to the result of Hunt[26] and the contraction coefficient was found to be $C_c = 0.58$.

Most recent studies have opted for a reduced contraction coefficient of $C_c = 0.58$ in the case of an axisymmetric orifice in an infinite plane, compared to the value of 0.61 for a two-dimensional slit in an infinite plane found by Kirchhoff[17] or Von Mises.[20] Nevertheless, the results provided by Von Mises[20] seem to be a good enough approximation for the axisymmetric three-dimensional case, all the more as the model does not account for any secondary effects such as gravity, viscosity, capillarity, or unsteadiness. Most importantly, Von Mises'[20] analytical results are readily available for all orifice-to-tube diameter ratios D_0/D_p and cone angles θ, and does not require any numerical computations. For these reasons, the analytical result of Von Mises[20] will be used in the present work to estimate the contraction coefficients of axisymmetric jets exiting orifices.

The objectives of the paper are twofold. First, a comprehensive parametric study of the influence of the geometrical parameter D_0/D_p on the production of the invariants of the motion is presented. For a given exhaust speed, the goal is to determine the influence of the orifice-to-tube diameter ratio D_0/D_p on the final production of the invariants of the motion. Second, a modified slug-flow model is proposed to account for the contraction imposed to the flow by the orifice plate.

The structure of the paper is as follows: In Sec. II, the slug-flow model is presented with, first, a review of the classic slug-flow model and, second, a description of the method used to estimate the value of the contraction coefficient. Then, the modified slug-flow model which incorporates the contraction of the flow is presented (Sec. II C). Section III presents the experimental conditions with some emphasis on the velocity program (Sec. III B) and the velocity profile measured at the exhaust (Sec. III C). Critical observations on the flow field at the exhaust are made in Sec. IV A. The modified slug-flow model is then compared to the measurements carried out at a fixed exhaust speed in Sec. IV B. In particular, the rate of change of the invariants of the motion is compared to the proposed model. The following Sec. IV C shows another set of measurements obtained at a fixed exhaust diameter-based Reynolds number and concludes on the validity of the model for the range of Reynolds numbers tested. Finally, the nonzero offset of the invariant of the motion at $t=0$ is explained by Krueger's[1,10–12] overpressure model in Sec. V and an extension to this model is proposed.

II. THE SLUG-FLOW MODEL

A. The classic slug-flow model

For an unbounded axisymmetric flow, the Euler equations possess a finite number of invariants associated with the symmetries of the equations. Among them, the kinetic energy corresponds to the invariance of the Euler equations to time while the hydrodynamic impulse corresponds to the invariance of the Euler equations to spatial displacement (provided that no non-conservative forces are applied to the domain). The invariance of circulation results from the degeneracy of the equations in two dimensions. For an unbounded axisymmetric flow with no swirl, and in a cylindrical coordinate system (x, r, θ), the aforementioned integrals of the motion read

$$\Gamma = \iint \omega \, \mathrm{d}r \, \mathrm{d}x, \tag{1}$$

$$I = \pi\rho \iint \omega r^2 \, \mathrm{d}r \, \mathrm{d}x, \tag{2}$$

$$E = \pi\rho \iint (u^2 + v^2) r \, \mathrm{d}r \, \mathrm{d}x, \tag{3}$$

where $\omega = \partial v/\partial x - \partial u/\partial r$ is the azimuthal vorticity and u and v are the axial and radial velocities, respectively.

Originally, the slug-flow model, as introduced by Didden,[6] aims at predicting the circulation generated at the lips of a sharp-edged nozzle. The model was extended by Gharib *et al.*[7] to estimate the hydrodynamic impulse and kinetic energy discharged by a parallel starting jet. The slug-flow model can be summarized as follows:

$$\mathrm{d}\Gamma_{slug} = \frac{1}{2} U_0^2 \mathrm{d}t, \tag{4}$$

$$\mathrm{d}I_{slug} = \frac{1}{4} \pi\rho U_0^2 D_0^2 \mathrm{d}t, \tag{5}$$

$$\mathrm{d}E_{slug} = \frac{1}{8} \pi\rho U_0^3 D_0^2 \mathrm{d}t. \tag{6}$$

For a thorough derivation, the reader is referred to the paper of Krieg and Mohseni.[3]

B. The contraction of the flow

When fluid is pushed through an orifice, the streamlines at the exhaust are bent toward the centerline and the flow detaches from the sharp edge to form a tube (or sheet) of fluid of reduced cross section called *vena contracta*. For a (rectilinear) two-dimensional flow, the contraction coefficient reduces to the ratio of the widths, whereas for an axisymmetric configuration, the contraction coefficient becomes $C_c = D_\star^2/D_0^2$, where $D_\star$ is the diameter of the *vena contracta* and D_0 is the diameter of the orifice (see Fig. 1). It was shown in previous literature that the result for the two-dimensional case is a fair approximation of the equivalent axisymmetric problem and the analytical results of Von Mises[20] for a two-dimensional conical slit in a channel of given width [Figs. 1(b) and 1(c)] can therefore be used to estimate the contraction a circular orifice is imposing to the flow.

A summary of Von Mises'[20] work is presented here. Computing the velocity potential of a steady inviscid incompressible irrotational plane flow is made feasible by the use of the complex potential $w(x + \mathrm{i}y) = \phi + \mathrm{i}\psi$, where ϕ is the velocity potential, ψ is the Lagrange stream function and x and y are the Cartesian coordinates. Finding the free streamline is therefore equivalent to finding the function $\zeta(w)$ which satisfies both equation $U_\star \mathrm{d}z/\mathrm{d}w = \zeta(w)$, where $U_\star$ is the freestream velocity, and the boundary conditions, which is performed by means of conformal transformations. It can be shown that solving the two-dimensional problem of a jet forming through a conical slot of angle $\theta = \pi\kappa$, as shown in Fig. 1, can be parametrized by the function $t^\kappa = 1/\zeta(w)$. The speed at infinity upstream is fixed by the parameter h^κ as

$$\frac{U_\star}{U_p} = \left(U_\star \frac{\mathrm{d}z}{\mathrm{d}w} \right)_\infty = \frac{1}{h^\kappa}, \tag{7}$$

and the contraction coefficient for the two-dimensional problem is therefore

$$C_c = \frac{A_\star}{A_0} = \frac{D_\star}{D_0} = \frac{U_p}{U_\star} \frac{D_p}{D_0} = \frac{h^\kappa}{D_0/D_p}, \tag{8}$$

with

$$\frac{D_0}{D_p} = 1 - \sin(\pi\kappa) \frac{l}{L} \tag{9}$$

and

$$\frac{l}{L} = \frac{h^\kappa}{\pi} \int_0^1 \frac{\mathrm{d}\xi}{\xi^\kappa} \left[\frac{1}{\xi + h} + \frac{1}{\xi + \frac{1}{h}} - \frac{2}{\xi + 1} \right]. \tag{10}$$

Note that there is no need to solve Eq. (8) for h. Instead, it can be assigned a value from 0 to 1 and the contraction coefficient C_c can be computed accordingly. For more details on the method, the reader is referred to the original papers[20] or the textbooks of Lamb,[13] Birkhoff and Zarantonello,[14] Gurevich,[15] or Batchelor.[16]

Equation (8) results in Fig. 2 and the precise numerical values for the cases investigated experimentally are given in Table I. For a nozzle case, the contraction coefficient is identically 1 as no contraction should occur when the tube is ending flush with the exhaust plane. For a 90° angle, Eq. (8) gives the contraction coefficient of a straight angle orifice [Figs. 1(a) and 1(b)]. Noteworthy is the possibility of having different cone angles which can either be applied to model converging

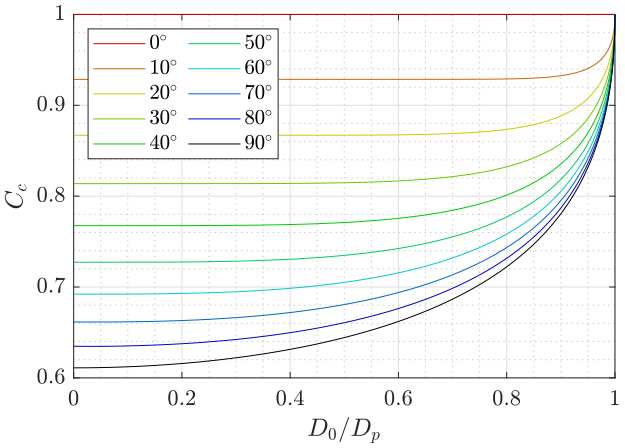

FIG. 2. Contraction coefficient as a function of the diameter ratio following the model of Von Mises.[20]

nozzles, such as the one used by Yu *et al.*,[28] Gao *et al.*,[29] or Rosenfeld *et al.*,[30] or model the presence of the orifice vortex upstream of the plate. Indeed, a recirculation region is expected to form ahead of the orifice plate, hence forcing the flow to exit with a nonnegligible radial component which can be accounted for by Von Mises'[20] model. Bear in mind that the size of this recirculation region is also expected to depend on the orifice-to-tube diameter ratio. Finally, the above Eq. (8) can be used to compute the contraction coefficient of an inverted conical nozzle, the limiting case being the mouthpiece of Borda with a contraction coefficient of 0.5 at the limit $D_0/D_p \to 0$.[18,19]

C. The modified slug-flow model

Using the conservation of mass (or volume), the geometric quantities (subscript 0) are related to the tube of fluid far downstream (subscript $\star$), the *vena contracta*, and, for an axisymmetric flow, the contraction coefficient is

$$C_c = \frac{A_\star}{A_0} = \frac{D_\star^2}{D_0^2} = \frac{L_0}{L_\star} = \frac{U_0}{U_\star}. \tag{11}$$

Making use of the contraction coefficient, a modified slug-flow model is introduced as

$$\mathrm{d}\Gamma_\star = \frac{1}{2} U_0^2 \mathrm{d}t \times 1/C_c^2, \tag{12}$$

$$\mathrm{d}I_\star = \frac{1}{4} \pi \rho U_0^2 D_0^2 \mathrm{d}t \times 1/C_c, \tag{13}$$

$$\mathrm{d}E_\star = \frac{1}{8} \pi \rho U_0^3 D_0^2 \mathrm{d}t \times 1/C_c^2. \tag{14}$$

Note that for a parallel starting jet, the contraction coefficient is 1, and the classic slug-flow model of Sec. II A is resumed.

Time is usually made non-dimensional using the exhaust quantities as $t^* = U_0 t/D_0$, where U_0 is the exhaust speed and D_0 is the diameter of the nozzle or orifice. This dimensionless time is usually referred to as *formation time* but the authors prefer the generic term of *non-dimensional time*. The present model suggests that the effective slug of fluid has a different shape and a non-dimensional time can be defined instead as $T^* = U_\star t/D_\star$. The latter is referred to as the *corrected non-dimensional time* or the *modified non-dimensional time*. A paper on the consequences of such a redefinition of the timescale on the formation number of orifice-generated vortex rings is available.[31]

III. MEASUREMENTS

A. Apparatus

Experiments are conducted in a water tank onto which a 101.6 mm inner diameter tube is mounted. 2.38 mm-thick aluminum plates with different orifice diameters are attached to the exhaust of the tube and the orifice-to-tube diameter ratios D_0/D_p are therefore 0.375(0.125)1.000, the end case being the straight tube without any plate. Water is continuously pushed out by a piston actuator sealed with rubber o-rings. The piston encoder provides the real-time position of the actuator. Moreover, the embedded PID controller of the piston was tuned beforehand in order to mitigate any spurious overshoot at the end of the acceleration period.

Time-resolved planar particle image velocimetry (PIV) is used to measure the velocity field at the exhaust. The field of view extends equally on each side of the axis of symmetry and is adjusted to visualize at least two diameters downstream of the exhaust. The vertical plane containing the axis of symmetry is illuminated with a high-speed Nd:YLF laser (LitronLaser LDY302 PIV Series). Recording is performed using a high-speed high-resolution CMOS camera (Photron FASTCAM Mini WX50). Both the laser and the camera are triggered by a digital delay generator (Stanford Research System DG645) and the frame rate is adjusted to the exhaust speed to comply with the requirements of maximum spatial displacement within the image plane for the PIV processing. For instance, for an exhaust speed of 100 mm s^{-1}, the frame rate is chosen to be 160 Hz. The PIV processing is performed using DaVis10 software (LaVision GmbH) which results in a 170 × 170 vector field with a spatial resolution between

TABLE I. Summary table of the experimental conditions performed at a fixed exhaust speed.

Orifice diameter	D_0/D_p	C_c (90°)	C_c (70°)	C_c (50°)	U_p (mm s^{-1})	$\bar{U}_p$ (mm s^{-1})	U_0 (mm s^{-1})	$\bar{U}_0$ (mm s^{-1})
4.0 in = 101.6 mm	1.000	1.000	1.000	1.000	100.00	99.867 ± 1.745	100.0	99.867 ± 1.745
3.5 in = 88.9 mm	0.875	0.762	0.779	0.805	≈76.56	76.401 ± 1.304	100.0	99.789 ± 1.703
3.0 in = 76.2 mm	0.750	0.703	0.727	0.765	56.25	56.070 ± 1.068	100.0	99.680 ± 1.898
2.5 in = 63.5 mm	0.625	0.667	0.698	0.745	≈39.06	38.864 ± 1.091	100.0	99.493 ± 2.793
2.0 in = 50.8 mm	0.500	0.644	0.681	0.735	25.00	24.792 ± 0.818	100.0	99.168 ± 3.271
1.5 in = 38.1 mm	0.375	0.629	0.670	0.730	≈14.06	13.889 ± 2.148	100.0	98.769 ± 15.272

0.90 and 1.8 mm, depending on the orifice plate, but always less than $0.02D_0$. More precisely, a four-pass cross correlation algorithm is used, ending in a 24×24 pixel interrogation window, with 50% overlap. The uncertainty in the velocity magnitude is estimated to be $0.01U_0$ on average. The derivatives of velocity in the axial and radial directions are computed using a finite-difference fourth-order Padé scheme. For more information on the experimental setup, the reader is referred to Limbourg and Nedić[5] or Limbourg.[32]

Two sets of measurements are performed to validate the proposed modified slug-flow model. In the first set of measurements, for all orifice-to-tube diameter ratios, the exhaust speed U_0 is kept constant, hence having a varying diameter-based Reynolds number $Re_{D_0} = U_0 D_0/\nu$, with values ranging from 3810 to 10 160 (see Table II). For a given stroke length L_0, or equivalently a given duration T_0, the stroke-based Reynolds number $Re_{L_0} = U_0 L_0/\nu$ is thus kept constant. In a second set of measurements, the diameter-based Reynolds number is fixed to $Re_{D_0} = 5080$ and the exhaust speed, or rather the piston speed, is modified accordingly (see Table III).

The total circulation, hydrodynamic impulse, and kinetic energy generated by the apparatus are measured in the control volume defined by the extent of the field of view whose boundaries are far enough from the exhaust to encompass the entire discharged quantities. The invariants of the motion are measured by means of Eqs. (1)–(3) within the top and bottom half-planes and each contribution is then averaged out to give a single value.

A total of 15 runs was taken for each orifice plate in both sets of measurements. The precise quantitative results are presented in Tables II and III, the uncertainty being the standard deviation over the 15 runs.

B. Velocity program

A step impulse velocity program was used for all orifice-to-tube diameter ratios. After a short period of acceleration of about 0.1 s the piston reaches a constant speed $\bar{U}_p$ with an uncertainty of less than 3%, except for the $D_0/D_p = 0.375$ case (see Table I). The uncertainty in the piston velocity is primarily due to the limited resolution of the position sensor of the actuator. For this reason, the nominal piston velocity program is presented in Fig. 3 alongside the normalized speed at the exhaust and at the centerline for different orifice-to-tube diameter ratios. Note that Fig. 3 presents the measured centerline velocity time history averaged over the 15 repeat PIV measurements. Additionally, a cubic spline interpolation function is used to smooth the experimental curves. A transient phase is observed for all orifice-to-tube diameter ratios, the ramp-up period being as large as the ratio D_0/D_p is close to 1. It was estimated to be the duration necessary to reach 95% of the final value, which is shown in Fig. 3. This initial ramp-up of the centerline speed is consistent with the theory of starting flows in pipes.[33] Moreover, a slight overshoot is visible which can be attributed to the presence of the leading vortex ring in the close vicinity of the exhaust which creates a surrounding velocity field pulling the fluid out of the orifice.

The slow ramp-up of the centerline velocity in the case of a nozzle has previously been reported by Krueger,[10] using the experimental data of Didden,[6] and by Krueger,[11] after numerically solving the viscid axisymmetric incompressible Navier–Stokes equations for a knife-edged nozzle. The boundary layer thickens in the tube which ultimately leads to a higher-than-expected centerline velocity. Furthermore, a bend in the centerline velocity was also reported in both cases without any physical explanation. As rightly pointed out by Krueger,[1] at the very first instants, the front of the material surface remains flat and the flow behaves like the potential flow in front of a circular translating disk. The flow then acts as a solid column of fluid and the exhaust centerline velocity follows the velocity program closely. After, the effect of the boundary layer becomes substantial and the centerline speed follows the expected ramp-up to eventually reach the value of the parabolic profile of a Poiseuille flow.

C. Velocity profile

The available experimental setup enables to take measurements at the exhaust and the velocity profile is shown for each orifice plate in Fig. 4. The measurements were taken for exhaust-based non-dimensional times $t^* = U_0 t/D_0$ between 2.5 and 3.0 and were then averaged out over time and over the 15 runs.

For the nozzle case, i.e., $D_0/D_p = 1.000$, the velocity profile is relatively "top-hat" as the flow inside the tube is not fully developed. The velocity profile starts from zero at the straight angle edge, i.e., at $r = D_0/2$, to reach the prescribed value at about $0.4D_0$. As expected, the radial velocity is zero and the velocity magnitude is essentially the axial velocity, in line with the classic slug-flow model. As time increases, the boundary layer inside the nozzle generator thickens which would ultimately produce a parabolic velocity profile. This is the correction Shusser *et al.*[8] and Dabiri and Gharib[9] proposed to incorporate to the slug-flow model.

For orifices, the velocity profile is far from uniform and extrema are visible at the edge of the plate. These velocity profiles are similar to those observed by Didden[6] who noted a large axial velocity near the edge of nozzles at small times, causing a large vorticity production and an increase in the overall circulation generated. In the case of orifices, the thickness of the boundary layer is minimal and both radial and axial velocities exhibit extrema at the edge of the exhaust throughout the formation process. Krieg and Mohseni[3] highlighted the effects of a nonzero radial velocity component on the integrals of the motion generated by non-parallel starting jets, and the present measurements complement their findings by investigating the influence of the orifice-

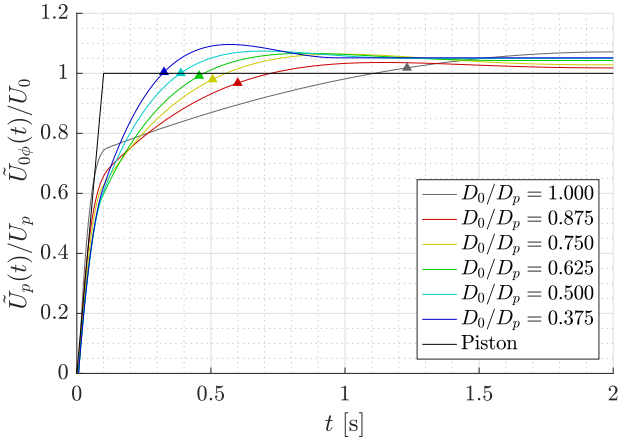

FIG. 3. Normalized piston velocity program and normalized measured centerline velocity at the exhaust for orifice-to-tube diameter ratios of $D_0/D_p = 0.375(0.125)1.000$ and for a fixed exhaust speed. Triangles correspond to the estimated delay.

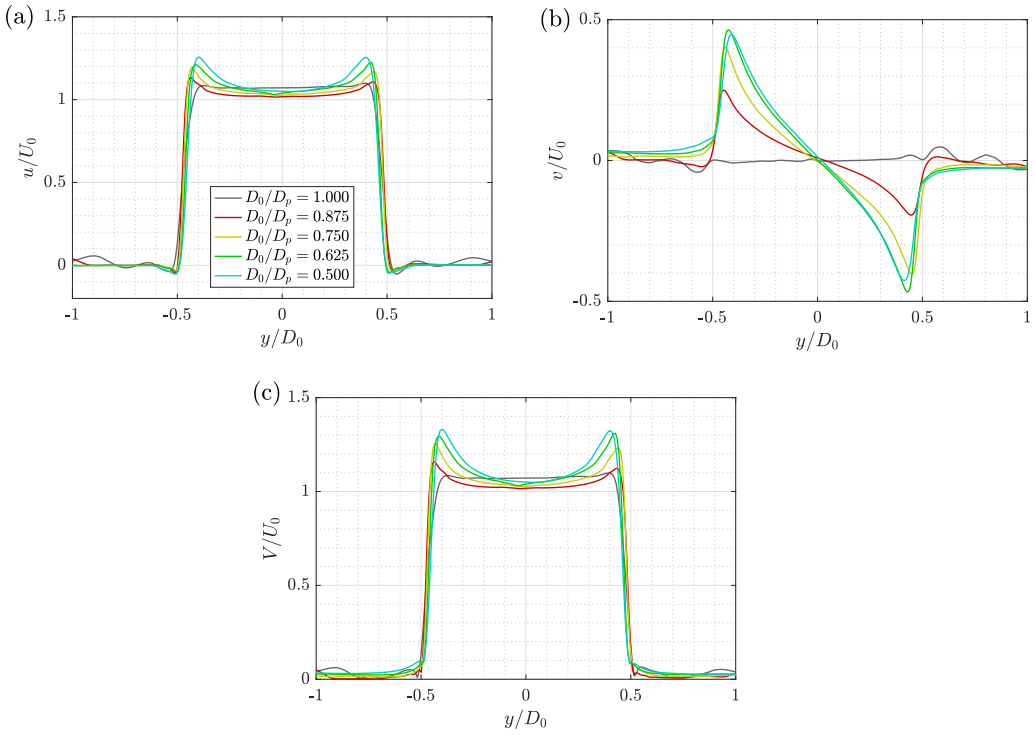

FIG. 4. Normalized velocity profile; (a) axial velocity, (b) radial velocity, (c) velocity magnitude for orifice-to-tube diameter ratios $D_0/D_p = 0.500(0.125)1.000$ and for a fixed exhaust speed.

to-tube diameter ratio on the flow field. From Fig. 4(b), it is found that the radial velocity increases as the ratio D_0/D_p reduces. In fact, it is found to reach $\pm 0.45U_0$ at a radial position of about $0.4D_0$ for orifice-to-tube diameter ratios of $D_0/D_p = 0.625$ and 0.500.

Finally, the velocity profile is measured to be narrower, with a magnitude higher than the target speed, and this for both the nozzle case and the orifice cases, which is in line with the presence of the flow contraction. Although the model of Von Mises[20] assumes the *vena contracta* to be reached at infinity downstream, here the increased speed is visible very close to the exhaust. Moreover, as stated above, the extrema of the velocity profile are observed at a location of about $0.4D_0$ which corresponds to the location of the free streamline of a jet exiting a tube with an orifice of ratio 0.5. Whether the contraction is due to the orifice plate only, or by the surrounding velocity field induced by the generated vortices, is unclear at this stage. The leading vortex ring being at a downstream position of one orifice diameter or greater (see Fig. 5), its influence on the exhaust kinematics is assumed to be limited and so the nonzero radial velocity can be attributed to the presence of the orifice plate only. Also, note that the influence of the orifice plate decreases downstream with a reduced radial velocity and an increased axial velocity, which nevertheless results in an increased velocity magnitude (not shown here); the leading vortex ring and the following train of vortices generate a surrounding velocity field similar to pipe flows. Finally, note that it was not possible to show the $D_0/D_p = 0.375$ case due to limitations in the experimental setup which prevented from resolving the flow near the orifice edge with enough confidence. Nevertheless, the centerline velocity presented in Fig. 3 was well-resolved.

IV. RESULTS AND DISCUSSION

A. Observations

Vorticity field snapshots at an exhaust-based non-dimensional time of $t^* = U_0 t/D_0 = 3.0$ are shown in Fig. 5(a) for the different orifice plates and with a fixed vorticity scale. Although the exhaust speed is chosen to be identical, hence having a fixed stroke-based Reynolds number, the nozzle geometry clearly shows a difference in the formation mechanism of the starting vortex; a continuous feeding shear layer remains attached to the leading vortex ring at least up to a non-dimensional time of $t^* = 3.0$, consistent with the findings of Gharib *et al.*[7] As the orifice diameter reduces in size, and the ratio D_0/D_p decreases, the feeding shear layer is replaced by a discrete train of vortices of relatively larger size compared to the leading vortex ring. This observation corroborates the study of Limbourg and Nedić[5] which highlighted this difference in vortex ring formation; the special boundary conditions of an orifice geometry force the flow to detach, similarly to vortex shedding, and an increased production of the invariants of the motion is observed.

Moreover, at an exhaust-based non-dimensional time of $t^* = 3.0$, the positions of the leading vortex rings are not the same for all cases, which shows that the formation processes of vortex rings emanating from different orifice-to-tube diameter ratios differ from one another. More precisely, the non-dimensional time $t^* = U_0 t/D_0$ does not accurately normalize the kinematics of vortex rings emanating from orifice geometries. However, the use of the modified slug-flow model and the non-dimensionalization of time by the corrected quantities, i.e., $T^* = U_\star t/D_\star$, brings all leading vortex rings at an axial position of about $x/D_0 = 1.0$. This illustrates the validity of the

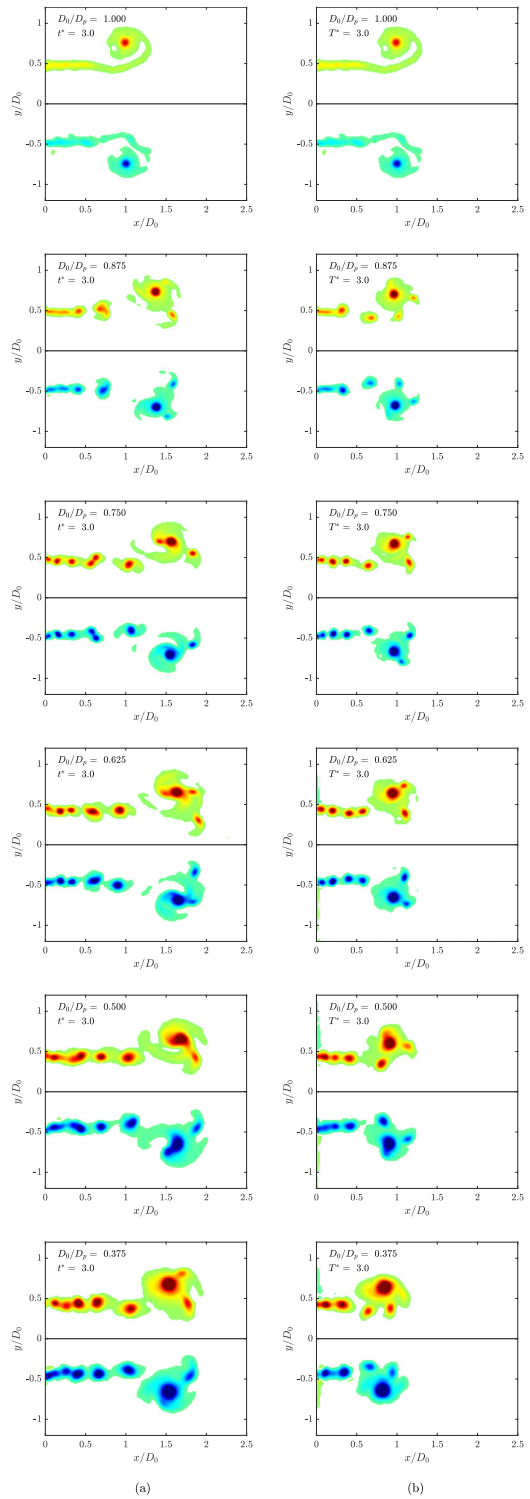

FIG. 5. Vorticity contours at orifice-to-tube diameter ratios of $D_0/D_p = 0.375(0.125)1.000$ for a fixed exhaust speed at (a) an exhaust-based non-dimensional time of $t^* = 3.0$ and (b) a corrected non-dimensional time of $T^* = 3.0$. Vorticity scale is the same for all contour plots.

timescale model proposed by Limbourg and Nedić[31] for orifice-generated vortex rings.

B. Invariants of the motion for a fixed exhaust speed

The time evolution of the measured invariants of the motion, as defined in Eqs. (1)–(3), are presented in their dimensional form in Figs. 6(a)–6(c), and this for a fixed target exhaust speed. Besides, the rate of change of the quantities is measured at large times, and compared to both the classic slug-flow model [Eqs. (4)–(6)] and the modified slug-flow model [Eqs. (12)–(14)] in Figs. 6(d)–6(f). Moreover, the contraction coefficient is computed using Von Mises'[20] method for three different cone angles in Eq. (8) which results in three different curves in Figs. 6(d)–6(f). The values of the contraction coefficients are reported in Table I and the raw results are reported in Table II.

Compared to the nozzle case, the orifice geometry is producing more circulation, and this for all orifice-to-tube diameter ratios [Fig. 6(a)]. Because the exhaust speed is kept constant, the classic slug-flow model predicts the same rate of production of circulation for all cases and $d\Gamma_{slug}/dt$, as defined in Eq. (4), is a constant. As shown in Fig. 6(d), although the classic slug-flow model is a fair approximation for the nozzle case with an 11% underestimation, the discrepancy with the model increases as the orifice-to-tube diameter ratio D_0/D_p decreases, to finally reach a value of about 2.3 times the classic slug-flow model for diameter ratios of 0.625, 0.500, and 0.375. This value is corroborated by Krieg and Mohseni[3] and Limbourg and Nedić.[5] On the other hand, the modified slug-flow model accurately predicts the increase in the circulation for decreasing orifice-to-tube diameter ratios D_0/D_p, with a maximum discrepancy of about 10% with the measurements (Table II). Nevertheless, the modified model fails at predicting the plateau and the slight reduction in the production rate of circulation for small D_0/D_p ratios.

Unlike circulation, the production of hydrodynamic impulse reduces as the size of the orifice decreases, and the nozzle geometry provides the largest impulse [Fig. 6(b)]. This is not surprising as, for a fixed exhaust speed, the volume of fluid discharged increases with increasing exhaust diameter, which is consistent with the classic slug-flow model presented in Eq. (5). The classic slug-flow model, however, does not properly estimate the latter decrease in impulse with decreasing orifice-to-tube diameter ratios. As shown in Fig. 6(e), the classic slug-flow model underpredicts the rate of production of impulse with a discrepancy reaching 50% for $D_0/D_p = 0.625$. Again, this corroborates observations made by Krieg and Mohseni[3] and Limbourg and Nedić.[5] Interestingly, not only does the modified slug-flow model better estimate the rate of production of the impulse with a maximum difference of 10% (Table II), but it also predicts that the production of impulse should reach a maximum at an orifice-to-tube diameter ratio of $D_0/D_p = 0.967$ for the 90° orifice case, the position of the extremum getting closer to $D_0/D_p = 1.000$ as the cone angle θ is reduced.

The evolution of the total kinetic energy is shown in Fig. 6(c). A surprising observation is that the cases with a ratio of $D_0/D_p = 0.875$ and 0.750 produce more energy than the nozzle case. This is counter-intuitive and against the classic slug-flow model, as the exhaust speed is fixed and the diameter of the discharged column of fluid is reduced, hence suggesting a monotonic decrease in kinetic energy with decreasing ratio D_0/D_p [Eq. (6)]. The modified slug-flow model, introduced in Eq. (14), appears to adequately predict the rate of production of kinetic energy with a maximum difference of 25% [Fig. 6(f) and

TABLE II. Summary table for the results obtained at a fixed exhaust speed.

D_0/D_p	U_0 (mm s^{-1})	Re_{D_0}	$d\Gamma/d\Gamma_{slug}$	dI/dI_{slug}	dE/dE_{slug}	$d\Gamma/d\Gamma_\star$	$dI/dI_\star$	$dE/dE_\star$
1.000	100.0	10 160	1.111 ± 0.010	0.964 ± 0.015	0.979 ± 0.013	1.111 ± 0.010	0.964 ± 0.015	0.979 ± 0.013
0.875	100.0	8890	1.531 ± 0.009	1.245 ± 0.014	1.381 ± 0.010	0.890 ± 0.005	0.950 ± 0.010	0.803 ± 0.006
0.750	100.0	7620	1.963 ± 0.009	1.384 ± 0.012	1.852 ± 0.011	0.969 ± 0.004	0.973 ± 0.009	0.914 ± 0.005
0.625	100.0	6350	2.279 ± 0.010	1.473 ± 0.023	2.143 ± 0.014	1.015 ± 0.004	0.983 ± 0.015	0.955 ± 0.006
0.500	100.0	5080	2.320 ± 0.008	1.449 ± 0.038	2.162 ± 0.018	0.963 ± 0.003	0.934 ± 0.024	0.898 ± 0.008
0.375	100.0	3810	2.244 ± 0.032	1.469 ± 0.054	1.903 ± 0.033	0.887 ± 0.012	0.924 ± 0.034	0.752 ± 0.013

Table II]. Again, a maximum in the production of kinetic energy is predicted by the modified slug-flow model at a ratio of $D_0/D_p = 0.910$ for the 90° angle orifice, and $D_0/D_p = 0.922$ and 0.938 for cone angles of 70° and 50°, respectively. This extremum is also visible in the measurements to a lesser extent suggesting the occurrence of other physical phenomena reducing the effect of the contraction at those large orifice-to-tube diameter ratios.

The existence of this extremum, for both the hydrodynamic impulse and the kinetic energy, is mathematically explained by the respective weight of the exhaust diameter and the contraction coefficient in Eqs. (13) and (14); the contribution of the contraction coefficient term starts dominating the exhaust diameter squared term at an orifice-to-tube diameter of 0.872 for the impulse, and 0.681 for the energy. The product then reaches a maximum at a ratio of 0.967 for the impulse and 0.910 for the energy, before returning to the classic slug-flow model value at $D_0/D_p = 1.000$, for which $C_c = 1.000$.

Overall, the classic slug-flow model, as defined in Eqs. (4)–(6), provides an adequate approximation of the rate of production of circulation, hydrodynamic impulse, and kinetic energy generated by a nozzle geometry with a difference of +11%, −4%, and −2%, respectively. The difference becomes substantial with orifice geometries with measurements reaching +130%, +50%, and +120% of the predicted value. The corrected slug-flow model, however, reduces drastically the differences, as shown in Table II.

In Figs. 6(d)–6(f), the modified slug-flow model curves were obtained with the contraction coefficient computed from the model of Von Mises[20] for a two-dimensional slit in a channel (Fig. 1). A coarser approach would be to use a fixed contraction coefficient of $C_c = \pi/(\pi + 2) \approx 0.611$, as was done by Krueger[10,12] to estimate the centerline speed at the exhaust of an orifice. Clearly, this is too coarse of an approximation. For instance, it would not account for the increase in production of circulation for decreasing D_0/D_p, and the model would give a constant value of about 134 cm^2 s^{-2} for all diameter ratios, value obtained with Von Mises'[20] model at $D_0/D_p = 0$ for which $C_c = 0.611$ [Fig. 6(d)].

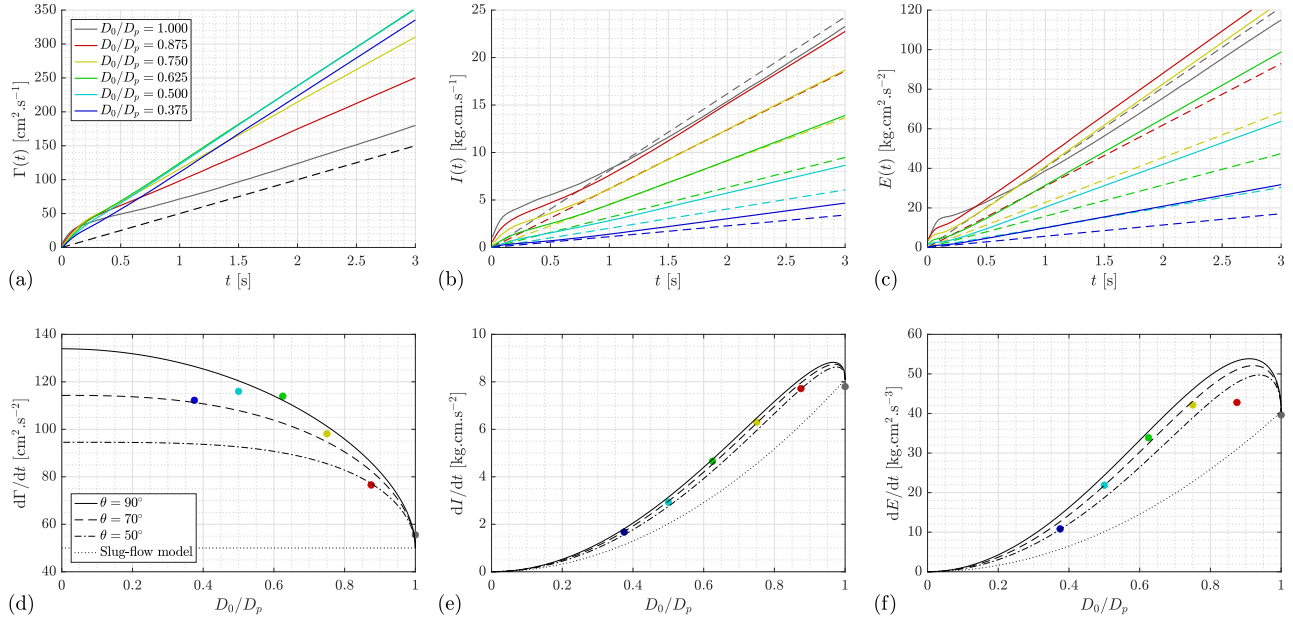

FIG. 6. Dimensional invariants of the motion; (a) circulation, (b) hydrodynamic impulse, and (c) kinetic energy as a function of time, measured for a fixed exhaust speed. The classic slug-flow model is shown as color-coded dashed line. Rate of production of the invariants of the motion; (d) circulation, (e) hydrodynamic impulse, and (f) kinetic energy as a function of the orifice-to-diameter ratio, measured for a fixed exhaust speed. The modified slug-flow model is shown as black lines for different cone angles. The classic slug-flow model is shown as a black dotted line.

TABLE III. Summary table for the results obtained at a fixed diameter-based Reynolds number.

D_0/D_p	U_0 (mm s^{-1})	Re_{D_0}	$d\Gamma/d\Gamma_{slug}$	dI/dI_{slug}	dE/dE_{slug}	$d\Gamma/d\Gamma_\star$	$dI/dI_\star$	$dE/dE_\star$
1.000	50.0	5080	1.170 ± 0.028	0.988 ± 0.029	0.980 ± 0.014	1.170 ± 0.028	0.988 ± 0.029	0.980 ± 0.014
0.875	57.1	5080	1.483 ± 0.017	1.194 ± 0.013	1.291 ± 0.009	0.862 ± 0.010	0.910 ± 0.010	0.751 ± 0.005
0.750	66.7	5080	1.915 ± 0.017	1.353 ± 0.019	1.774 ± 0.018	0.945 ± 0.008	0.951 ± 0.013	0.876 ± 0.009
0.625	80.0	5080	2.252 ± 0.012	1.478 ± 0.018	2.093 ± 0.017	1.004 ± 0.006	0.987 ± 0.012	0.933 ± 0.008
0.500	100.0	5080	2.330 ± 0.008	1.432 ± 0.023	2.160 ± 0.015	0.968 ± 0.003	0.923 ± 0.015	0.897 ± 0.006
0.375	133.0	5080	2.334 ± 0.048	1.361 ± 0.026	2.053 ± 0.045	0.923 ± 0.019	0.856 ± 0.016	0.812 ± 0.018

Finally, although the plate covering the exhaust of the tube has a geometrical 90° angle, the presence of an eventual orifice vortex ahead of the plate can be accounted for by the present model. Indeed, the recirculation region upstream of the plate modifies the angle at which the fluid is discharged, and this can be modeled by changing the angle of the conical slit in Eq. (8) [Fig. 1(c)]. This is valid provided that the two-dimensional results apply to the axisymmetric case, which, in view of the results of Salamatov,[24] seems reasonable. Compared to the modified model, Figs. 6(d)–6(f) show a relative decrease in the measured rate of production of the invariants when the ratio D_0/D_p decreases below 0.500 (see also the three last column of Table II). This can be attributed to the presence of a more pronounced recirculation region upstream of the orifice plate which reduces the effective angle of the orifice. As show in Figs. 6(d)–6(f), using a different cone angle θ in Eq. (8) when computing the contraction coefficient results in a better estimation of the invariants of the motion for small orifice-to-tube diameter ratios. In particular, the use of a 70° cone angle enables to predict accurately the production of circulation for a ratio of $D_0/D_p = 0.375$. Moreover, the use of the contraction coefficient of a 50°-angle conical slit enables to accurately predict the values for both the hydrodynamic impulse and the kinetic energy at a ratio $D_0/D_p = 0.375$. This also highlights a limitation of the present model as a single value for the cone angle cannot predict accurately the rate of production of all three quantities at a given orifice-to-tube diameter ratio. Furthermore, for a given invariant of the motion, a single cone angle does not fit all measurement points. This is quite expected as the size of the recirculation region upstream of the plate is a function of the orifice depth, i.e., the orifice-to-tube diameter ratio D_0/D_p.

C. Invariants of the motion for a fixed Reynolds number

The above results were presented for a fixed exhaust speed of $U_0 = 100\,\text{mm s}^{-1}$, hence a fixed unit-stroke-based Reynolds number

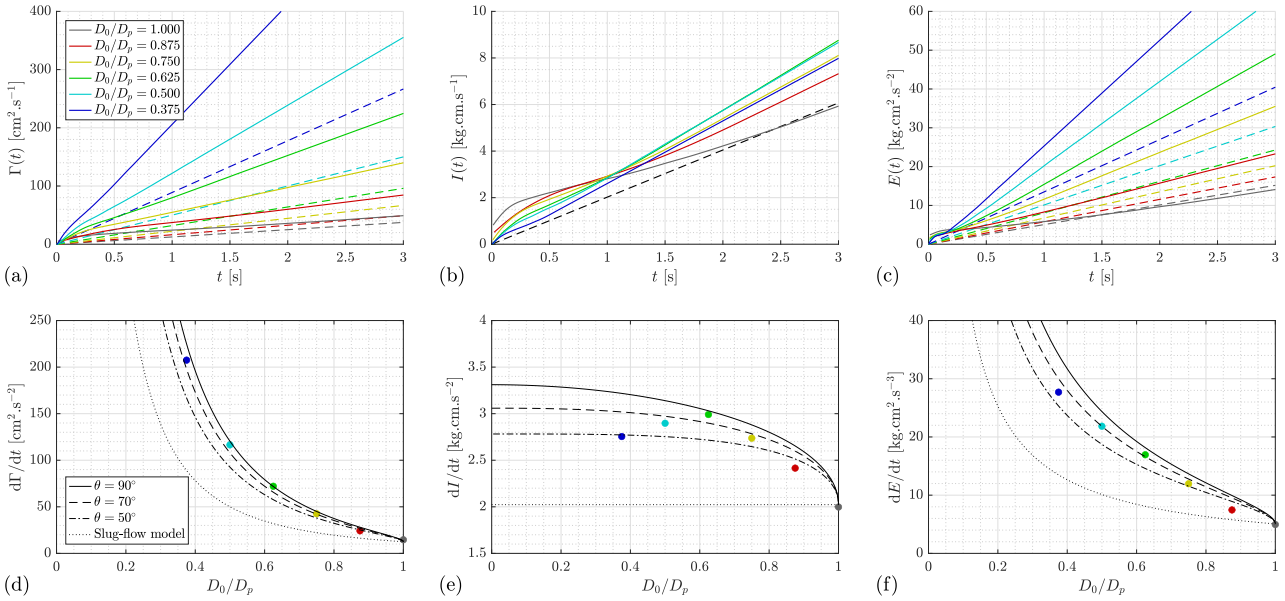

FIG. 7. Dimensional invariants of the motion; (a) circulation, (b) hydrodynamic impulse, and (c) kinetic energy as a function of time, measured for a fixed diameter-based Reynolds number. The classic slug-flow model is shown as color-coded dashed line. Rate of production of the invariants of the motion; (d) circulation, (e) hydrodynamic impulse, and (f) kinetic energy as a function of the orifice-to-diameter ratio, measured for a fixed diameter-based Reynolds number. The modified slug-flow model is shown as black lines for different cone angles. The classic slug-flow model is shown as a black dotted line.

$Re_{L_m=1}$. As suggested by the modified slug-flow model, the effective column of fluid has a reduced diameter and a larger speed, the difference with the exhaust quantities, subscript 0, being as large as the contraction coefficient is small. When aiming for a fixed exhaust speed U_0, the Reynolds number Re_{D_0} based on the outlet diameter naturally changes with the orifice diameter. Therefore, the observations made in Sec. IV B can *a priori* be a diameter-based Reynolds number effect. This section presents measurements carried out at a fixed diameter-based Reynolds number of $Re_{D_0} = 5080$, hence adapting the target exhaust speed to the change in diameter (Fig. 7 and Table III).

As predicted by the classic slug-flow model, the rate of production of circulation increases as the orifice diameter decreases because the exhaust speed is increasing inversely proportionally to the diameter [Fig. 7(a)]. Again, the rate of production is underestimated by the classic slug-flow model, as shown in Fig. 7(d), with a measured rate reaching 2.3 times the predicted value for $D_0/D_p = 0.625$, 0.500, and 0.375. Modeling the contraction of the flow using Von Mises'[20] results for a 90°-angle plate enables to accurately estimate the production of circulation with a maximum error of 10% for $D_0/D_p = 0.375$ and $D_0/D_p = 0.875$ (Table III).

As shown in Figs. 7(b) and 7(e), the production of hydrodynamic impulse increases with decreasing orifice-to-tube diameter ratio to reach a value 50% larger than the classic slug-flow model value at a ratio of $D_0/D_p = 0.625$. For lower diameter ratios of $D_0/D_p = 0.500$ and 0.375, the production rate decreases; normalized by the classic slug-flow model, the rate of production of impulse displays the same trend as in Sec. IV B (see the fifth column of Tables II and III). The modified slug-flow model, however, reduces the discrepancy with a maximum difference of 15% for $D_0/D_p = 0.375$.

Finally, the kinetic energy increases with decreasing diameter ratio as the exhaust speed increase inversely proportionally to the decrease in orifice diameter [Fig. 7(c)]. Again, as in Sec. IV B, the corrected slug-flow model provides a superior estimate of the production rate, with differences of less than 25% for all orifice cases, compared to an underestimation reaching 120% with the classic slug-flow model [Fig. 7(f) and Table III].

To summarize, the results obtained at a fixed diameter-based Reynolds number demonstrate the ability of the modified slug-flow model to estimate the rate of production of the invariants of the motion independently of the Reynolds number, whether one uses the definition of the Reynolds number in terms of the stroke length or in terms of the exhaust diameter (see Tables II and III). Furthermore, although not shown here for the sake of brevity, measurements were taken at a fixed orifice-to-tube diameter of $D_0/D_p = 0.500$ and exhaust speeds ranging from 75 to 500 mm s^{-1}. These measurements are made available in Limbourg.[32] Again, the modified slug-flow model was found to accurately estimate the production of the invariants of the motion, hence demonstrating the validity and the applicability of the model over a wide range of Reynolds numbers.

V. INITIAL OFFSET

After a short transient period, the invariants of the motion follow a linear trend which can be fitted at large times, say greater than 1 s, and from which the value of the quantities at the origin can be found. For instance, the measured circulation is expressed as $\Gamma = m_\Gamma t + p_\Gamma$, where m_Γ is the production rate, labeled $\mathrm{d}\Gamma/\mathrm{d}t$, and shown in Figs. 6(d) and 7(d), and $\Gamma_p \equiv p_\Gamma$ is the initial offset. The results are shown as circle symbols in Fig. 8 for a fixed exhaust speed and in Fig. 9 for a fixed diameter-based Reynolds number. Interestingly, the circulation offset increases linearly as the orifice-to-tube diameter ratio increases, even though the nozzle case is observed to have a lower offset value [Figs. 8(a) and 9(a), circles]. This trend in the measured circulation offset suggests that for small D_0/D_p ratios, a negative offset in circulation would be obtained. This is attributed to the time delay observed in the exhaust velocity, estimated to be the duration at which the centerline velocity reaches 95% of its final value, marked in Fig. 3 by color-coded symbols. After modifying the time origin to incorporate this delay, the measured circulation offsets are shifted vertically as shown in Figs. 8(a) and 9(a) (triangles). In the limit of a zero orifice-to-tube diameter ratio, the circulation offset would now be zero, which is physically consistent.

This offset may have different origins. Krueger[1,10–12] proposed an overpressure correction to the slug-flow model in order to take into account the rise of pressure during the unsteady forcing. Making use of the vorticity transport equation for incompressible flows, Krueger[10] expressed the additional circulation due to overpressure as $\Gamma_p = U_0 D_0/c$ where $c = \pi$ for knife-edged nozzles and $c = 2$ for orifices in an infinite plane. In short, the unsteady contribution of pressure was related to the velocity potential at the centerline by the unsteady Bernoulli equation. As a first estimation, the velocity potential of a translating circular disk was used, leading to the coefficient $c = \pi$ [blue dotted line in Figs. 8(a) and 9(a)]. For an orifice in an infinitely large vessel, i.e., for $D_0/D_p \to 0$, the analytical expression of the velocity potential at the exhaust was calculated and its value at the centerline was found close to $c = 2$ (Ref. 34) [red dotted line in Figs. 8(a) and 9(a)]. Note that because Krueger's[1,10–12] model is only valid in the limit of zero orifice-to-tube diameter ratios, the red dotted curves are shown up to $D_0/D_p = 0.3$ in Figs. 8(a) and 9(a). The overpressure correction of Krueger,[10] which assumes a step increase in circulation at time zero, is shown in its original form in Figs. 8(a) and 9(a) as blue dotted and red dotted lines. The model is also adapted to account for the contraction of the flow by replacing the exhaust quantities (subscript 0) by the contracted quantities (subscript $\star$). The impact of the contraction coefficient on the overpressure correction is observed to be relatively small [blue solid and red solid lines in Figs. 8(a) and 9(a)].

The initial offsets for the hydrodynamic impulse and kinetic energy hover about zero (circles). When accounting for the time delay, the offset of these two quantities becomes substantial, especially for orifice-to-tube diameter ratios close to 1 (triangles). Most importantly, the offset increases in a power-law fashion, with a zero offset for a zero diameter ratio. Following the line of argument of Krueger,[1] the initial offset in impulse and energy can be explained by the overpressure effect and estimated by the same model. Making use of the velocity potential of a translating disk the additional hydrodynamic impulse is estimated by $I_p = 1/6\rho D_0^3 U_0$ and the kinetic energy by $E_p = 1/6\rho D_0^3 U_0^2$. The results are presented in Figs. 8(b) and 9(b) and in Figs. 8(c) and 9(c) as blue dotted lines. Krueger's[1,10–12] model accurately accounts for the "power-law-like" increase in the impulse offset and energy offset for increasing orifice-to-tube diameter ratios, but clearly underpredicts their absolute value. Again, it is possible to incorporate the contraction of the flow to the model of Krueger,[1,10–12] which is shown in Figs. 8 and 9 as blue solid lines. The impact of the contraction coefficient on the overpressure hydrodynamic impulse and kinetic energy is again minimal.

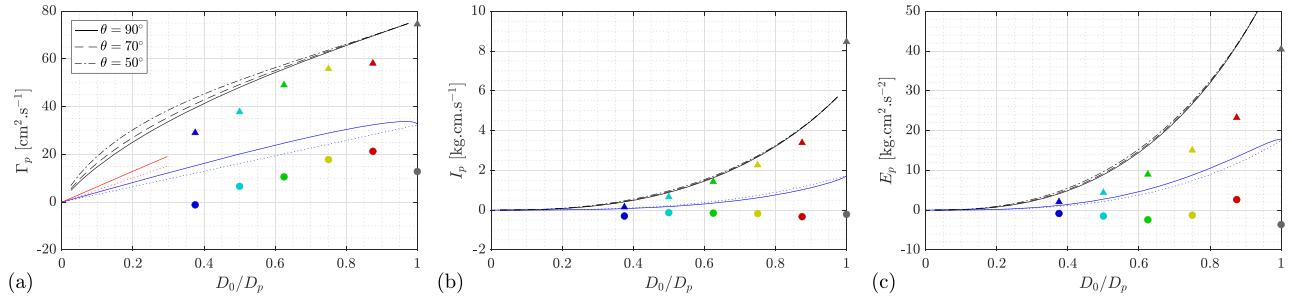

FIG. 8. Offset of the dimensional invariants of the motion; (a) circulation, (b) hydrodynamic impulse, and (c) Kinetic energy as a function of the orifice-to-diameter ratio, measured for a fixed exhaust speed. Triangles show the value of the offset after taking into account the time delay. The numerical results are shown as black lines. Overpressure model of Krueger;[1,10–12] blue dotted line $\Gamma_p = U_0 D_0/\pi$, $I_p = 1/6\rho D_0^3 U_0$, $E_p = 1/6\rho D_0^3 U_0^2$; blue solid line $\Gamma_p = U_\star D_\star/\pi$, $I_p = 1/6\rho D_\star^3 U_\star$, $E_p = 1/6\rho D_\star^3 U_\star^2$; red dotted line $\Gamma_p = U_0 D_0/2$; red solid line $\Gamma_p = U_\star D_\star/2$.

Note that the approach of Krueger[10,12] to model the velocity potential at the exhaust at the very first instant by the one of a translating circular disk was motivated by the observation that the front of the material surface during the rapid flow initiation is nearly flat. Nevertheless, this model assumes the presence of a velocity magnitude maximum at the edges, which is also observed in orifice starting flows (Fig. 4), and one may argue that this model is also applicable to the cases of orifices. Overall, the overpressure model of Krueger[1] predicts the general increase in the initial offset for increasing orifice-to-tube diameter ratios, although it does not account for the ratio *per se*, but only for the exhaust diameter. As such, Krueger's model[1,10–12] cannot differentiate straight nozzles of increasing exhaust diameter from orifices of increasing orifice-to-tube diameter ratios.

It is clear from Figs. 8(a) and 9(a) that the presence of an orifice increases the contribution of overpressure on circulation by forcing the flow to converge through the orifice. The model of Krueger[1,10–12] is derived from first principles and seems to be an appropriate methodology for estimating the initial offset in the circulation, the hydrodynamic impulse, and the kinetic energy by means of the velocity potential:

$$\Gamma_p = -\phi(0,0), \tag{15}$$

$$I_p = -2\pi\rho\int_r \phi(0,r) r\,\mathrm{d}r, \tag{16}$$

$$E_p = -2\pi\rho\int_r \phi(0,r) U_0(r) r\,\mathrm{d}r = U_0 I_p. \tag{17}$$

Using the velocity potential of a translating circular disk for estimating the velocity potential at the exhaust of the orifice seems to be too coarse of an approach. For this reason, computations of the velocity potential inside the tube were undertaken using the software FreeFEM v4.7.[35] Finding the velocity potential in the tube comes back to solving the Laplace equation $\nabla^2\phi = 0$ with pure Neumann boundary conditions. Specifically, the problem was solved on a domain representing the top half of the tube, of radius $D_p/2$ and length $1.5D_p$. The left inlet boundary condition was chosen to be the piston speed $\partial\phi/\partial x = U_p = (D_0/D_p)^2 U_0$ and the right outlet boundary condition was chosen to be the prescribed exhaust speed $\partial\phi/\partial x = U_0$. The no-penetration condition $\partial\phi/\partial r = 0$ was imposed on the outer wall and at the centerline, as well as on the orifice plate covering the exhaust $\partial\phi/\partial x = 0$. Because the Laplace equation subject to pure Neumann boundary conditions is only solvable up to a constant, the condition of having a zero velocity potential on the centerline at the farthest upstream location was enforced (red circle in Fig. 10). This condition is motivated by the fact that, in the case of an infinitely large vessel, the velocity potential reduces to zero at infinity upstream.[10] Moreover, this condition selects a velocity potential from the infinite number of solutions in the same manner for all orifice-to-tube diameter ratios,

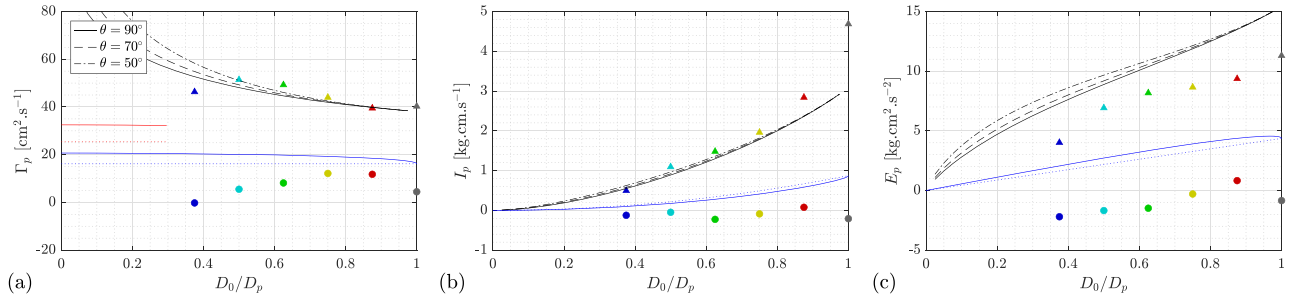

FIG. 9. Offset of the dimensional invariants of the motion; (a) circulation, (b) hydrodynamic impulse, and (c) kinetic energy as a function of the orifice-to-diameter ratio, measured for a fixed diameter-based Reynolds number. Triangles show the value of the offset after taking into account the time delay. The numerical results are shown as black lines. Overpressure model of Krueger;[1,10–12] blue dotted line $\Gamma_p = U_0 D_0/\pi$, $I_p = 1/6\rho D_0^3 U_0$, $E_p = 1/6\rho D_0^3 U_0^2$; blue solid line $\Gamma_p = U_\star D_\star/\pi$, $I_p = 1/6\rho D_\star^3 U_\star$, $E_p = 1/6\rho D_\star^3 U_\star^2$; red dotted line $\Gamma_p = U_0 D_0/2$; red solid line $\Gamma_p = U_\star D_\star/2$.

whether they are formed at a fixed exhaust speed or at a fixed diameter-based Reynolds number.

Figure 10 shows the numerical result for an orifice-to-tube diameter ratio of $D_0/D_p = 0.25$ and the overpressure circulation, hydrodynamic impulse, and kinetic energy, computed following the method of Krueger,[1,10–12] are shown as black solid lines in Fig. 8 for a fixed exhaust speed and Fig. 9 for a fixed diameter-based Reynolds number. The numerical results show overall good agreement with the experiment after correcting for the time delay (triangles). In particular, the model accurately predicts the increase in the overpressure circulation for a fixed target exhaust speed, and the decrease in the quantity for a fixed diameter-based Reynolds number, and this for increasing orifice-to-tube diameter ratios [Figs. 8(a) and 9(a)]. Besides, the numerical results also predict the increase in impulse and energy offsets for increasing D_0/D_p. More precisely, the numerical results accurately estimate the values of the overpressure hydrodynamic impulse, and this for both fixed exhaust speed and fixed diameter-based Reynolds number, the differences in the prediction being the highest for the nozzle case [Figs. 8(b) and 9(b)]. Finally, modeling the potential flow inside the tube accurately predicts the trend of the increasing kinetic energy initial offset, but fails at estimating the exact values. In particular, for a fixed target exhaust speed, the numerical results show a "power-law-like" increase whereas for a fixed diameter-based Reynolds number, the steady increase in the overpressure kinetic energy is well accounted for [Figs. 8(c) and 9(c)].

For completeness, the computations were undertaken for cone angles of 50° and 70°. As shown in Figs. 8 and 9, the influence of the cone angle θ on the overpressure quantities remains minimal for all orifice-to-tube diameter ratios and one may use the 90° curves to estimate the overpressure circulation, hydrodynamic impulse, and kinetic energy.

VI. CONCLUDING REMARKS

The influence of the orifice-to-tube diameter ratio D_0/D_p was investigated experimentally using time-resolved PIV, and this for both a fixed unit-stroke-based Reynolds number $Re_{L_m=1}$, i.e., fixed exhaust speed U_0, and a fixed diameter-based Reynolds number Re_{D_0}. In addition to the invariants of the motion, namely, the circulation, the hydrodynamic impulse, and the kinetic energy, the velocity profile was measured at the exhaust, as well as the time history of the exhaust centerline speed. A clear difference between the nozzle geometry and the orifice geometry was observed; whereas in the nozzle case the velocity profile remains flat in the radial direction with a negligible radial component of velocity, the velocity profile of orifice geometries presents extrema close to the edge of the orifice, owing to both the axial and radial components of velocity. These extrema are as pronounced as the orifice-to-tube diameter ratio is small. Besides, the time history of the centerline velocity shows a timescale associated with the initial ramp-up of the flow speed, the time delay being as large as the ratio D_0/D_p tends to 1. This delay was estimated as the duration required to reach 95% of the final value.

Furthermore, snapshots of the vorticity field obtained at a fixed exhaust-based non-dimensional time of $t^* = U_0 t/D_0 = 3.0$ and a fixed corrected non-dimensional time of $T^* = U_\star t/D_\star = 3.0$ show that non-dimensionalizing time by the corrected speed and diameter enables to collapse the dynamics of the leading vortex ring. This confirms the findings of Limbourg and Nedić[31] who showed that the

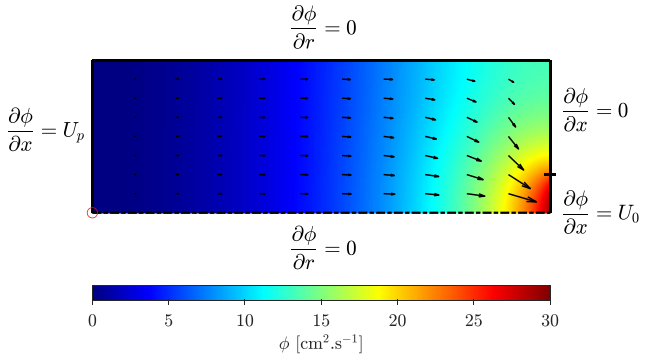

FIG. 10. Domain of computation and numerical solution for an orifice-to-tube diameter ratio of $D_0/D_p = 0.25$ and a cone angle of $\theta = 90°$.

modified slug-flow model can be used to unify the formation number of orifice-generated vortex rings with the one found for nozzles[36]

Also, the slug-flow model was revisited to account for the contraction of the flow in the case of orifices. The two-dimensional model of Von Mises[20] for a jet exiting a conical slot in a channel was used to predict the contraction coefficient of the present three-dimensional axisymmetric starting jet. The modified slug-flow model was proved to accurately estimate the rate of production of the invariants of the motion with discrepancies of less than 10% for the circulation. Most importantly, for a fixed target exhaust speed, the model suggests the existence of a maximum in the rate of production of hydrodynamic impulse and kinetic energy which weakly depends on the cone angle. Experimentally, this maximum was not reached, but an increased production of energy was still observed for $D_0/D_p = 0.875$. This paves the way for further investigations to find the most efficient way of forming starting jets.

Moreover, the validity of the model was tested against the exhaust speed, the diameter-based Reynolds number being kept constant at 5080 in a second set of measurements. It was shown that the modified slug-flow model accurately predicts the production rate of the invariants of the motion, and this independently of the target exhaust speed, at least in the range of speed considered in this study. To summarize, the present correction to the slug-flow model enables to accurately estimate the rate of production of the invariants of the motion for different orifice-to-tube diameter ratios, and appends to the classic slug-flow model for parallel starting jets. Additionally, it can be used to model the influence of the radial component of velocity on the production rate of the integrals of the motion by tuning the cone angle depending on the size of the recirculation region upstream of the orifice plate.

Finally, the overpressure correction of Krueger[1,10–12] was used to estimate the positive offset at $t = 0$ in the production of the invariants of the motion. This simple model, based on potential theory, enabled us to predict the increase in the additional overpressure invariants of the motion as the ratio D_0/D_p gets closer to 1. The model of Krueger,[1,10–12] which assumes the starting flow to behave as a circular translating disk, was extended to account for the different orifice-to-tube diameter ratios. Numerical computations were undertaken to estimate the velocity potential at the orifice exit of a pipe. Results showed overall good agreement with the experimental measurements corrected for the time delay.

ACKNOWLEDGMENTS

Financial support from the Natural Sciences and Engineering Research Council of Canada, Grant No. NSERC RGPIN-2017–04079, and the Fonds de Recherche du Québec Nature et Technologie, Grant No. 287771, are gratefully acknowledged.

DATA AVAILABILITY

The data that support the findings of this study are available from the corresponding author upon reasonable request.

REFERENCES

[1]P. S. Krueger, "The significance of vortex ring formation and nozzle exit over-pressure to pulsatile jet propulsion," Ph.D. thesis (California Institute of Technology, 2001).
[2]A. Glezer and M. Amitay, "Synthetic jets," Annu. Rev. Fluid Mech. **34**, 503–529 (2002).
[3]M. Krieg and K. Mohseni, "Modelling circulation, impulse and kinetic energy of starting jets with non-zero radial velocity," J. Fluid Mech. **719**, 488–526 (2013).
[4]M. Krieg and K. Mohseni, "A new kinematic criterion for vortex ring pinch-off," Phys. Fluids **33**, 037120 (2021).
[5]R. Limbourg and J. Nedić, "Formation of an orifice-generated vortex ring," J. Fluid Mech. **913**, A29 (2021).
[6]N. Didden, "On the formation of vortex rings: Rolling-up and production of circulation," Z. Angew. Mech. Phys. **30**, 101–116 (1979).
[7]M. Gharib, E. Rambod, and K. Shariff, "A universal time scale for vortex ring formation," J. Fluid Mech. **360**, 121–140 (1998).
[8]M. Shusser, M. Gharib, M. Rosenfeld, and K. Mohseni, "On the effect of pipe boundary layer growth on the formation of a laminar vortex ring generated by a piston/cylinder arrangement," Theor. Comput. Fluid Dyn. **15**, 303–316 (2002).
[9]J. O. Dabiri and M. Gharib, "A revised slug model boundary layer correction for starting jet vorticity flux," Theor. Comput. Fluid Dyn. **17**, 293–295 (2004).
[10]P. S. Krueger, "An over-pressure correction to the slug model for vortex ring circulation," J. Fluid Mech. **545**, 427–443 (2005).
[11]P. S. Krueger, "Circulation of vortex rings formed from tube and orifice openings," in Fluids Engineering Division Summer Meeting (2006), pp. 97–104.
[12]P. S. Krueger, "Circulation and trajectories of vortex rings formed from tube and orifice openings," Phys. D **237**, 2218–2222 (2008).
[13]H. Lamb, *Hydrodynamics* (Cambridge University Press, 1932).
[14]G. Birkhoff and E. H. Zarantonello, *Jets, Wakes, and Cavities* (Academic Press, Inc., 1957).
[15]M. I. Gurevich, *The Theory of Jets in an Ideal Fluid* (Pergamon Press Ltd., 1966).
[16]G. K. Batchelor, *An Introduction to Fluid Dynamics* (Cambridge University Press, 1967).
[17]G. Kirchhoff, "Zur theorie freier flüssigkeitsstrahlen," J. Reine Angew. Math. **70**, 289–298 (1869).
[18]J. C. de Borda, "Mémoire sur l'écoulement des fluides par les orifices des vases," Hist. Acad. R. Sci. **1766**, 579–607.
[19]H. von Helmholtz, "Über diskontinuierliche flüssigkeits-bewegungen," Akad. Wiss. Berlin **1868**, 215–228.
[20]R. Von Mises, "Berechnung von ausflußund überfallzahlen," Z. VDI **61**, 447–452 (1917); **61**, 469–474 (1917); **61**, 493–498 (1917).
[21]E. Trefftz, "Über die kontraktion kreisföormiger flüssigkeitsstrahlen," Z. Math. Phys. **64**, 34–61 (1916).
[22]R. V. Southwell and G. Vaisey, "Relaxation methods applied to engineering problems. XII. Fluid motions characterized by 'free' stream-lines," Philos. Trans. R. Soc. London A. **240**, 117–161 (1946).
[23]H. Rouse and A.-H. Abul-Fetouh, "Characteristics of irrotational flow through axially symmetric orifices," J. Appl. Mech. **17**, 421–426 (1950).
[24]D. Salamatov, "Flow of liquid from an infinitely long axially symmetric container," J. Appl. Math. Mech. **23**, 508–519 (1959).
[25]P. R. Garabedian, "Calculation of axially symmetric cavities and jets," Pacific J. Math. **6**, 611–684 (1956).
[26]B. W. Hunt, "Numerical solution of an integral equation for flow from a circular orifice," J. Fluid Mech. **31**, 361–377 (1968).
[27]R. W. Jeppson, "Inverse formulation and finite difference solution for flow from a circular orifice," J. Fluid Mech. **40**, 215–223 (1970).
[28]S. C. M. Yu, A. W. K. Law, and J. J. Ai, "Vortex formation process in gravity-driven starting jets," Exp. Fluids **42**, 783–797 (2007).
[29]L. Gao, S. C. M. Yu, J. J. Ai, and A. W. K. Law, "Circulation and energy of the leading vortex ring in a gravity-driven starting jet," Phys. Fluids **20**, 093604 (2008).
[30]M. Rosenfeld, K. Katija, and J. O. Dabiri, "Circulation generation and vortex ring formation by conic nozzles," J. Fluids Eng. **131**, 091204 (2009).
[31]R. Limbourg and J. Nedić, "An extension to the universal time scale for vortex ring formation," J. Fluid Mech. **915**, A46 (2021).
[32]R. Limbourg, "Formation of orifice-generated vortex rings," Ph.D. thesis (McGill University, 2021).
[33]G. Szymanski, "Quelques solutions exactes des équations d'hydrodynamique du fluide visqueux dans le cas d'un tube cylindrique," J. Math. Pures Appl. **11**, 67–108 (1932).
[34]A typo was found in the original publication of Krueger[10] and one should read J_1 instead of J_0 in the denominator of Eq. (28).
[35]F. Hecht, "New development in FreeFem++," J. Numer. Math **20**, 251–265 (2012).
[36]Making use of the modified slug-flow model, the critical non-dimensional numbers for vortex ring formation are $\alpha = E/(\rho^{1/2}\Gamma^{3/2}I^{1/2}) = \sqrt{\pi/2}\,(L_0(t)/D_0)^{-1} \times C_c^{3/2}$, $\beta = \Gamma/(\rho^{-1/3}I^{1/3}U_0^{2/3}) = 1/(2\pi)^{1/3}\,(L_0(t)/D_0)^{1/3} \times C_c^{-5/3}$, and $\gamma = V_0/(\rho^{-3/2}\Gamma^{-3/2}I^{3/2}) = 1/\sqrt{2\pi}\,(L_0(t)/D_0) \times C_c^{-3/2}$. Unlike stated in the original paper (Ref. 31), the non-dimensional quantities do depend on the contraction coefficients. As such, the slug-flow model shown in Fig. 2 of Ref. 31 corresponds to the classic slug-flow model for which $C_c = 1$. For a corrected version of the paper, one is referred to Limbourg.[32]